Quantitative hematocrit measurement of whole blood in a point-of-care lateral flow device using a smartphone flow tracking app

Eric Frantz, Hua Li, Andrew J. Steckl [*]

Nanoelectronics Laboratory, Department of Electrical Engineering and Computer Science, University of Cincinnati, Cincinnati, OH, 45221-0030, USA

A B S T R A C T

We present a rapid and quantitative point-of-care (PoC) system based on a smartphone application that is capable of accurately tracking the flow of red blood cells (RBCs) through a no-reaction lateral flow assay (nrLFA) device. Utilizing only the camera feed from the smartphone and built-in image processing, the nrLFA is identified and RBC fluid flow distances and rates are recorded in parallel with the test without the need of any custom hardware or enclosure. We demonstrated the application by first measuring and then calculating hematocrit (Hct) values of whole blood samples with nominal content of 28%, 35%, 40%, and 45% Hct on the nrLFA platform. The PoC system was able to accurately measure (to within 1% Hct of nominal values) whole blood Hct in ∼10–20 s after sample dispensing.

1. Introduction

Lateral flow immunoassay (LFIA) technology has been the driving force behind the development of simple and low-cost diagnostic tests with favorable characteristics, such as easy operation, rapid detection and high portability (Bahadır and Sezgintürk, 2016; Koczula and Gallotta, 2016; Sajid et al., 2015). In 1976, the first homemade LFIA test was performed as a pregnancy test to detect the human chorionic gonadotropin (hCG) hormone in urine (Bahadır and Sezgintürk, 2016). Today tens of millions of these tests are utilized as home pregnancy test kits worldwide (Insights, 2016). Currently, major applications of LFIA tests are the detection of antigens, antibodies, biomarkers (Steckl and Ray, 2018), cells, toxins, pathogens (Han et al., 2018), pesticides, heavy metals (Zhan et al., 2016), drugs, as well as products of gene amplification (Rohrman et al., 2012) in either qualitative or quantitative format. Compared to laboratory equipment or point-of-care (POC) digital analyzers, the advantages of LFIA tests include low cost, long shelf life, simple fabrication and easy operation (Li et al., 2017). A typical LFIA test strip (O'Farrell, 2009) consists of a series of overlapping membranes: cellulose sample pad for sample collection, fiber glass conjugate pad for conjugate release, nitrocellulose membrane for bioaffinity reaction between antibody and antigen, and cellulose wicking pad for flow assurance. The strip is usually placed inside a plastic housing to ensure flow consistency and easy handling. Lateral flow takes place within the hydrophilic porous materials through which fluid samples are transported due to capillary action without an external force. The structure (pore size, tortuosity, etc.) and composition (material substrate, density, surface additives, etc.) of each strip component is important to obtain high test sensitivity and specificity. A wide variety of components can be found in analyte samples, including ions, small molecules (proteins, etc.), and large components, such as cells and bacteria (Li et al., 2017).

A second category of lateral flow assays (LFAs) utilizes the transport properties of a fluid sample within porous materials as a result indicator of diagnostic tests, rather than the line-forming affinity reaction between antibody and antigen in immunoassays. These types of LFA tests primarily include blood grouping (Guan et al., 2014; Khan et al., 2010; Noiphung et al., 2015), hematocrit (Hct) measurement (Berry et al., 2016) and coagulation analysis (Hegener et al., 2017; Li et al., 2014, 2018a,b). They typically utilize whole blood as the sample fluid, and analyze the travel distance of a red color front (caused by the presence of red blood cells, RBCs) as a result indicator of the diagnostic tests (Li and Steckl, 2018). These types of LFA tests are further discussed in the last part of the Introduction section.

While the LFA test is very low cost, easy to use, robust, and adaptable it does have two major challenges. Conventional stand-alone LFA devices provide a qualitative result and are primarily used for "yes/no" tests. The other challenge is susceptibility to user interpretation of the test. Differences in test conditions (such as ambient lighting) and the medical condition of the test taker can result in different readings and/or

---

interpretations of the same test.

To overcome the limitations of the conventional LFA, diagnostic systems have been developed that measure <u>and</u> display the result to the user as a "yes/no" response or with specific quantitative data (Sajid et al., 2015; van Amerongen et al., 2018; Vashist et al., 2015). Quantitative LFA measurement systems can be classified into two categories: desktop systems designed to be used in a lab setting, and point-of-care (PoC) systems designed to be mobile and used in a range of environments. Desktop systems are already a mature technology, with several commercial readers available (AbingdonHealth, 2019; Axxin, 2019). These systems utilize high resolution imaging to record colorimetric or fluorescent images of LFA and LFIA test strips. The images are then analyzed and converted into quantitative measurements of test and control line intensities through software either on the reader, or on a connected computer system. The ubiquitous test lines in LFIAs have enabled these systems to detect a wide range of analytes using only colorimetric and fluorescent imaging (Sajid et al., 2015).

PoC systems are highly mobile and are typically handheld. In this article, we focus on smartphone-based PoC systems. The widespread use of smartphones, their built-in screen, processing capability, connectivity, and built-in sensors (such as the camera) make them an ideal platform for PoC systems (Kanchi et al., 2018). These systems can be divided into three categories based on how they utilize the smartphone: (1) as processor and user interface (UI), (2) as power supply for the measurement hardware, (3) to perform the measurement itself. The first category of systems typically performs the LFA measurement using some form of external hardware that then transmits the data, either wirelessly or through a USB connection to the smartphone for analysis and display to a user. An example is the use of the smartphone processor and UI diagnostics to interpret and display data from a piece of hardware that measures an iron status biomarker (serum ferritin) (Srinivasan et al., 2018). The second approach, smartphone powered, drives the measurement hardware from the phone itself and does not require additional power sources, allowing the test to be more mobile. Similar to the first category, smartphone powered PoC systems can also utilize the smartphone's display and processing capabilities. Power has been transmitted from a smartphone to PoC measurement hardware using the headphone port (Laksanasopin et al., 2015), USB port (Deng et al., 2016; Ghosh et al., 2020; Zhang et al., 2015), and NFC (Escobedo et al., 2019; Venkatraman et al., 2016) of the smartphone.

The third category of smartphone enabled PoC systems utilizes the hardware of the smartphone itself to perform the measurement. This style of PoC is the simplest and most common system used in conjunction with LFAs and typically utilizes the built-in camera in smartphones to capture images of the LFIA, then perform image analysis to determine signal strength (Eltzov et al., 2015). This category can be further divided into measurement systems with or without additional hardware. Unlike the measurement accessories discussed in the previous section, additional hardware discussed in this section only assists in taking measurements, but does not perform the measurement. External hardware is typically used to hold the LFA in a fixed position and provide a controlled lighting environment. The hardware used varies from rigid 3D printed structures (Hou et al., 2017) to paper-based holders (Yang et al., 2017). Diagnostic systems without additional hardware perform measurements with the smartphone's camera alone (Ding et al., 2018; Erenas et al., 2019) and typically rely more on the user to provide alignment. Without an enclosure, these applications needed to compensate for changes in ambient lighting. Additionally, without the test strip held into a fixed position, alignment becomes crucial for accurate colorimetric measurements. To solve alignment problems techniques, such as alignment marks (Lopez-Ruiz et al., 2014) and barcodes (Guan et al., 2014), have been used. One notable example of a commercial hardware-free smartphone-based PoC to measure LFIAs is the Novarum, (2018) system. Novarum uses images of LFIA tests to record and track test results for a variety of LFIA tests and only requires a smartphone application.

1.1. Basic approach

Our approach utilizes a smartphone-based lateral flow tracking application (LFTA) to measure whole blood flow through a no-reaction lateral flow assay (nrLFA). Similar to the approach used to detect whole blood glucose (Erenas et al., 2019), the LFTA utilizes the camera available on most commercial smartphones with no additional hardware to measure whole blood Hct. This allows handheld use (Fig. 1a), or the usage of a simple and low cost commercial smartphone stand (Fig. 1b). Image processing performed by the application enables the dynamic detection of an nrLFA cassette onto which blood samples are dispensed. The application's user interface consists of the following: display window, travel distance ("Distance"), test time ("Time"), hematocrit measurements ("Hct %" as discussed below), and a "button" to start or stop the test. Blood flow distance is extracted from a live video stream from the camera and shown in the display window. The test is started and stopped by the user, with all measured and calculated values stored locally on the smartphone after test completion. Detection of the cassette is required for blood flow measurements and is indicated on the display by the appearance of a green outline surrounding the cassette image. Additionally, outlines for the observation window (blue) and blood flow extent (red) are highlighted on the display window. If the cassette becomes misaligned during measurement, the test pauses until the user realigns the cassette. This prevents the recording of inaccurate test data caused by misalignment. In this approach, the application determines the flow distance based on the area of detected flow. This approach provides resilience to changes in lighting conditions as opposed to color intensity based distance measurements (Erenas et al., 2019).

The LFTA is designed for the automatic flow tracking and distance measurement of RBCs on the nrLFA device. Reported by the Steckl group (Hegener et al., 2017; Li et al., 2014, 2017, 2018a,b), the nrLFA device is a simplified version of conventional LFIA, consisting of fiber glass sample pad, nitrocellulose analytical membrane and cellulose wicking pad, but without a conjugate pad. While the main purpose of the nrLFA device is *in vitro* blood coagulation analysis (Hegener et al., 2017; Li et al., 2014, 2018a,b), the same device also exhibits great sensitivity in distinguishing whole blood with different Hct values (Li et al., 2017, 2018a,b). It was reported (Li et al., 2017) that by measuring the travel distance of RBCs or plasma on the nrLFA, the device is able to differentiate between citrated blood samples with Hct values of 25%, 30%, 35% and 40% without overlap in travel distances (mean ± standard deviation). When utilized for whole blood Hct measurement on the nrLFA device, the LFTA first identifies the rectangular shape (highlighted with a green rectangle in Fig. 1a of the plastic cassette regardless of the background color. After finding the cassette, the LFTA locates the rectangular observation window (highlighted with a light blue rectangle in Fig. 1a within the cassette outline. Following sample dispensing, the RBC front starts to appear in the observation window. The LFTA then detects the red color of the RBCs and creates a bounding rectangle (red rectangle in Fig. 1a around the blood flow. The LFTA then automatically performs real-time measurements of the length of red rectangle, which is the travel distance of RBCs on the nrLFA device. Last but not the least, the Hct value is automatically calculated using the relationship between Hct and RBC flow rate discussed above. Examples of changes in RBC flow distance as a function of Hct for a fixed time point of 150 s are shown in Fig. 1c. The measurement time, RBC distance and calculated Hct value is then displayed in real-time on the user interface with minimal delay. All RBC distances, calculated Hct values, and corresponding times are then saved in a text file to the phone memory.

Work by Kim et al., (2017) has previously demonstrated a quantitative smartphone-based PoC system to measure blood hematocrit values with a microfluidic chip. In their approach, they utilized a custom microfluidic chip to create a colorimetric test of Hct value in whole blood. The microfluidic chip was attached to a smartphone via a custom enclosure and analyzed using the smartphone's camera. In contrast, our approach does not require any custom hardware unique to the
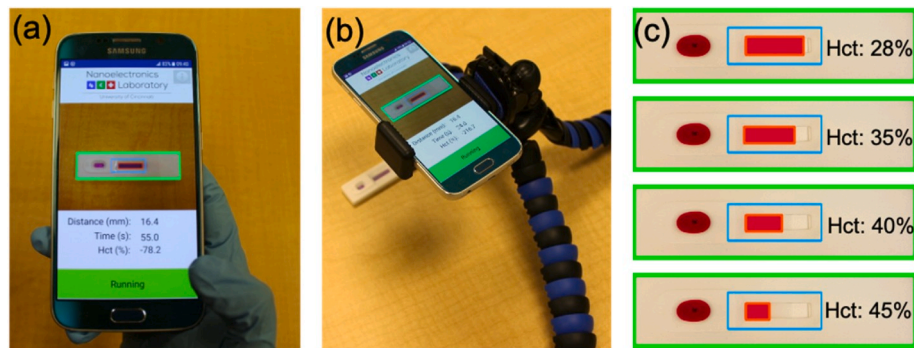
Fig. 1. Operation of LFTA on commercial smartphone with fluid flow measurements taken by hand (a) and utilizing a smartphone stand (b). Illustration of RBC flow distance for different Hct levels after a fixed test time of 150 s (c).

application. Additionally, our flow based Hct test using a nrLFA is less sensitive to changes in lighting than colorimetric analysis.

2. Methods

2.1. Detection principle

Hematocrit calculation is performed using measured blood flow distance and flow time starting from the time when blood flow is detected in the observation window. Blood flow distance is determined on each video frame using the five-step process shown in Fig. 2, with each step further detailed in the supplemental material. The first step is the identification of the LFA cassette through color masking and contour detection. Next, the observation window position is determined based on the size and position of the detected cassette. The blood flow within the observation window is then detected. Blood flow distance (in mm) is extracted from the window length (16.5 mm) and the measured pixel value. The blood flow distance and current test time is used to calculate the Hct value (as discussed above) for each recorded camera frame. The

Hct value is displayed to the user after a specific delay time after blood flow first appears in the observation window and is updated at 1.0 s intervals. The Hct value is no longer calculated after the blood flow reaches the end of the observation window, or the time exceeds 180 s. The application was written in Java using Android Studio 2.3.3 and all image processing and manipulation was done using the OpenCV 3.2 libraries. All testing was done on a Samsung Galaxy s7.

2.2. Hct value calculation algorithm

The travel distance of the RBC front through the nrLFA membrane can be approximated using the Lucas-Washburn model (Li et al., 2014). Equation (1) shows the Lucas-Washburn equation, where L is the length of the fluid front in a porous medium, γ is the surface tension of the fluid, θ is the water contact angle of the porous media, r is the radius of the capillary tubes in the porous media, μ is the dynamic viscosity of the fluid, and t is the fluid travel time within the porous medium.
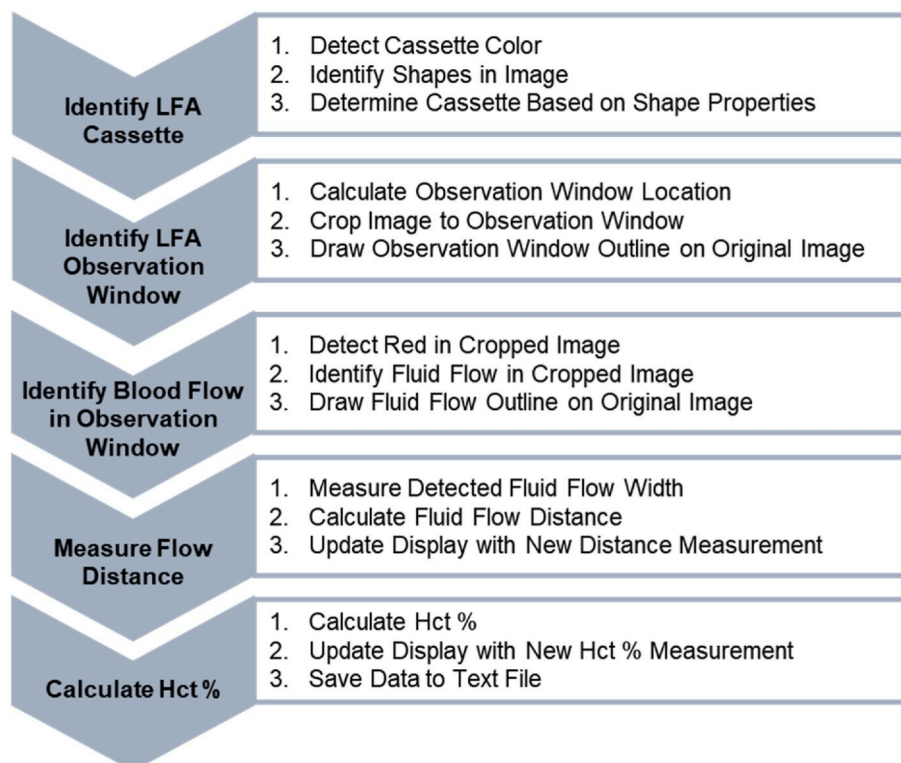

Fig. 2. Flow chart outlining the per-frame process used to extract fluid flow distance and calculate Hct.

$$L^2 = \frac{\gamma \cos(\theta) r}{2\mu} t \tag{1}$$

In the case of the nrLFA used, the fluid is whole blood and the porous medium is a nitrocellulose membrane. The equation shows a square root dependence between travel distance, and both viscosity and time. Based on this relationship and our experimental data (Fig. 6b) we can calculate the Hct value as a function of both time and distance. Because of the range of our viscosity values (for Hct between 28% and 45%) we are able to use a linear approximation between Hct and blood flow distance (d_{bf}) as shown in equation (2a). The square root time dependence of travel distance as a function of time is taken into account in the equation as a time dependence of the slope ($a(t)$) and the y-intercept $b(t)$. Both $a(t)$ and $b(t)$ are second order polynomial functions whose coefficients are extracted through curve fitting performed on the calibration test set. To obtain the Hct value based on test time and blood flow distance, equation (2a) is solved for Hct (equation (2b)):

$$d_{bf}(t) = Hct * a(t) + b(t) \tag{2a}$$

$$Hct = \frac{d_{bf}(t) - b(t)}{a(t)} \tag{2b}$$

2.3. Blood sample preparation

Testing of the LFTA was performed using citrated rabbit blood with Hct values of 35%, 40%, and 45%, in line with previous work done by Li et al., (2017) Hct values of 35%, 40%, and 45% were obtained by removing plasma from low Hct citrated rabbit blood (measured at 28% Hct as received from the vendor). Plasma was removed from 1 mL of citrated rabbit blood after light centrifuging (Thermo Fisher Scientific accuSpin Micro 17, Osterode am Harz, Germany) at 500 g for 8 min. 200 μL, 300 μL and 378 μL of plasma was separately removed per blood sample to create citrated rabbit blood with 35%, 40% and 45% Hct, respectively. The samples were then re-mixed through light agitation. Hct values both before and after modification were measured using a microhematocrit centrifuge (LW Scientific Zipocrit, Lawrenceville, GA). 100 μL of citrated blood with various Hct (28%, 35%, 40% and 45%) was dispensed onto the fluid reservoir of nrLFA device to initiate the flow measurement using LFTA phone application, and the measurements were repeated 6 times for each Hct value (n = 6).

3. Results and discussion

3.1. Background noise elimination results

To determine the ability of cassette recognition, the LFTA was tested with the nrLFA placed on several different backgrounds. Fig. 3 highlights detection on colorful backgrounds with circular shapes (Fig. 3a) and varying sized rectangular shapes (Fig. 3b). Measurement of 28% Hct blood was performed at a distance of 12 cm between cassette and smartphone. The successful detection of the cassette indicated that correct color masking and contour setting were used in cassette detection.

Detection of the nrLFA cassette on noisy backgrounds allows the LFTA to remain accurate despite the testing environment. Test results also demonstrate the restriction of color detection to the area within the detected LFA. Changes in background color or shape did not affect the detection of cassette and observation window, nor the calculation of blood flow distance and Hct.

3.2. Accuracy testing

Accurate measurement of the fluid flow distance is essential for measurement of Hct. To achieve this the distance measurement must be accurate at all ranges. Determination of flow distance based on maximum measured cassette length could lead to measurement error between the two extreme cases (zero distance and maximum distance). To determine accuracy of LFTA distance measurements, 100 μL of Hct 40% citrated rabbit blood was used to perform tests (n = 3) with the blood flow distance being recorded via LFTA while also being manually measured using precision calipers. The smartphone was fixed 12 cm above the LFTA using a phone stand (Fig. 1b). Comparison between manual measurements and those by the video application allow us to detect inaccuracies in distance detection that may be caused by the algorithm or the smartphone. Fig. 4 shows the average values of blood flow distances measured through the LFTA (with standard deviation) and all manually measured data points.

The manual measurements deviated from the average LFTA measured values by at most ~0.7 mm, or approximately 2 × the average standard deviation of LFTA values. This could be the result of the LFTA resolution, but it is more likely caused by measurement error in the manual measurements. The overall trend of the manually recorded data matches closely with the LFTA recorded data. These results show that our LFTA is capable of accurately measuring fluid flow distance from the start of the test strip to its end.
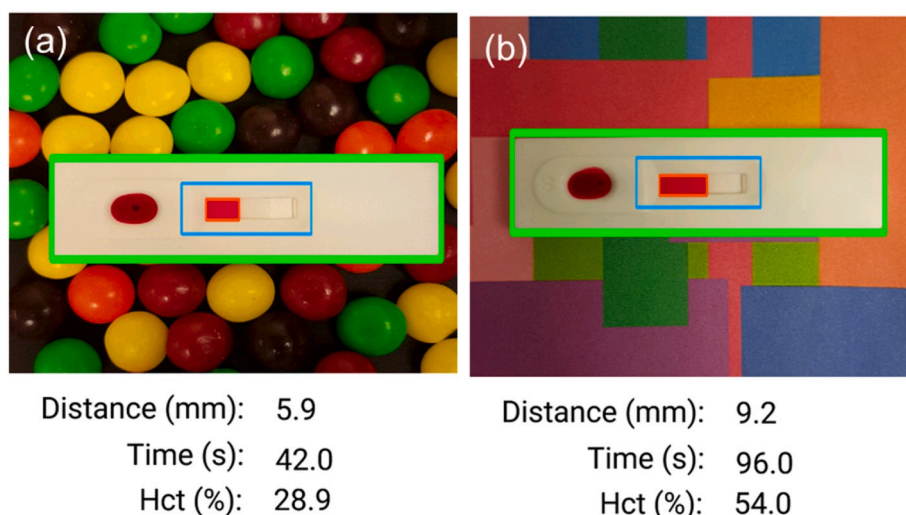

Fig. 3. Detection of nrLFA cassette, fluid flow distance, and Hct on colorful backgrounds with circular shapes (a) and varying sized rectangles (b).
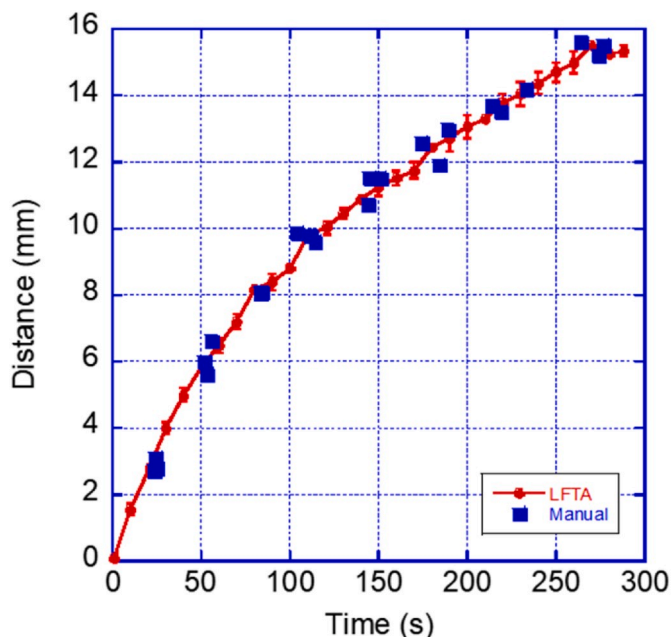
Fig. 4. Flow distance of 40% Hct citrated rabbit blood obtained by manual (blue points) and automated measurements performed with the LFTA (red points, standard deviation and line). (For interpretation of the references to color in this figure legend, the reader is referred to the Web version of this article.)

3.3. Human reproducibility/consistency testing

Distance measurements were performed with nine independent users in order to establish *handheld* accuracy, user consistency, and cross user variability. A red dye solution was substituted for blood due to its high flow rate and easy repeatability. Users were asked to use the LFTA to measure and record red dye flow through the nrLFA cassettes three times each, for a total of 27 (n = 27) tests. Red dye was prepared by dissolving 5g powder Keyacid Red XB 100% dye into 10 mL of DI water. Fig. 5a shows the user-recorded flow distance measured by the LFTA at 10 s intervals for each test performed by each user. The average user measurement and associated standard deviation (SD) (Fig. 5b) is shown for each test time between t = 10s and t = 100s, with the height of each column representing the average value.

These results show a standard deviation ranging from ~10.5% to 1.3% (Fig. 5b). The highest SD of 10.5% (0.48 mm) is measured at 20 s across all users and tests. The SD is seen to decrease as test time increases, reaching 1.3% at 100s. The decrease in standard deviation as a function of time is most likely the result of the resolution of the smartphone's camera. At short times and corresponding small flow distances, the measurement error caused by the minimum resolution of the smartphone camera represents a greater percentage of the overall fluid flow distance than for longer flow distances, causing greater deviation at the initial phases of testing. The standard deviation in flow rates caused by the test itself is also mirrored in the measurement results of the LFTA. The minimum measurement distance's dependence on smartphone camera resolution shows that the application may take longer (require longer flow distances) to measure distance on lower end phones. However, it also shows that, as smartphone camera quality increases each year the application as the potential for faster, more accurate results.

A key difficulty with smartphone video measurements, including flow-based measurements, is ensuring that variations in the distance between the smartphone and the test strip introduced by handheld operation do not affect the measurement accuracy or precision. As discussed in the introduction, many video measurements of LFIA operation typically utilize custom hardware to hold the LFIA strip a fixed distance
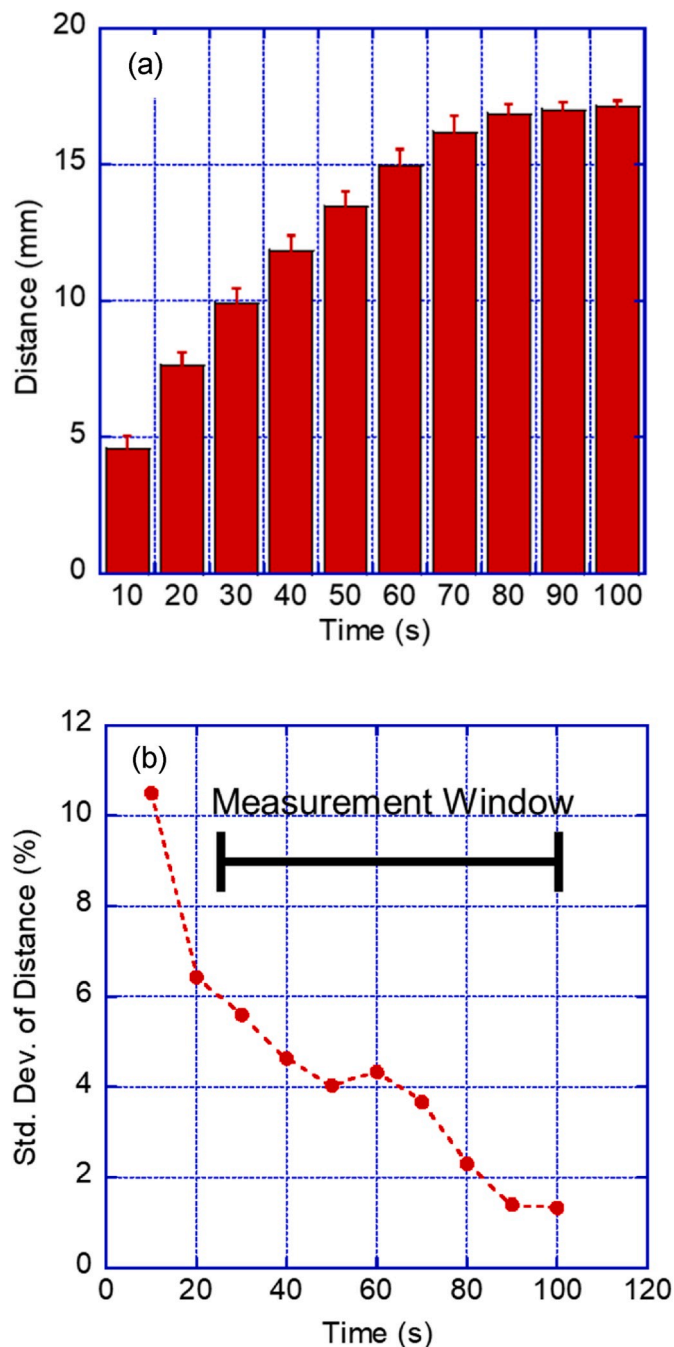

Fig. 5. LFTA user variability measurements from 9 different users with 3 tests each (n = 27): (a) average values; (b) standard deviation of user test results in percentage of current flow distance, with the LFTA measurement window outlined in black.

from the smartphone. The low measurement error observed across multiple users shows that the LFTA's adaptive fluid flow calculation is successfully compensating for these variations, without the use of external hardware.

3.4. Hematocrit measurement

Citrated rabbit blood samples with Hct values of 28 (as received), 35, 40, and 45% were prepared as described above and tested multiple times (n = 6) with nrLFAs at each Hct percentage. The LFTA was used to measure and record the blood flow distance as a function of time for each Hct value. During testing the smartphone was secured at a distance
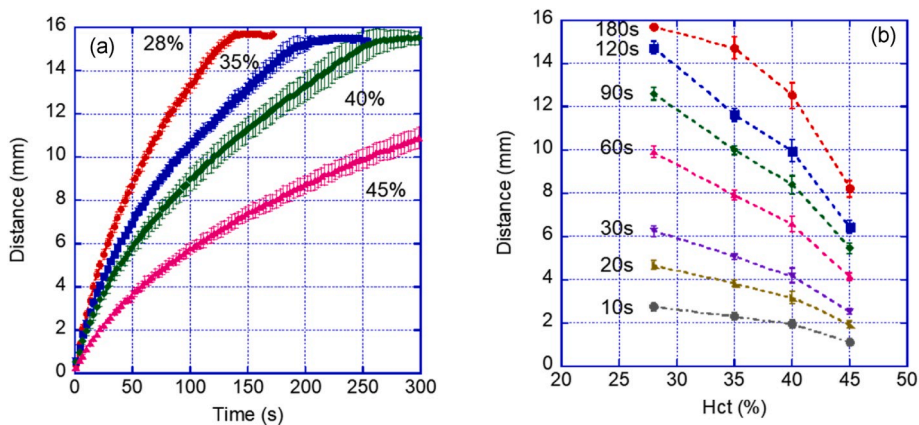
Fig. 6. Measurement of blood flow travel distance for citrated rabbit blood with HCT values of 28, 35, 40, and 45% as a function of: (a) time at fixed Hct %; (b) Hct% for fixed transport time.

of 12 cm above the nrLFA cassette using a phone stand. The average measured distance is shown as a function of time in Fig. 6a and the calculated Hct is shown in Fig. 6b. The trend of higher Hct values causing slower flow rates is consistent with previous reports (Berry et al., 2016).

A linear regression was created for each curve in Fig. 6b and used to calculate the values of coefficients a(t) and b(t) in Eq. (2). The LFTA algorithm was then used to calculate Hct values from the collected data spanning a period of 180 s. Fig. 7a shows the *calculated* Hct for each test

in Fig. 6a. The overlap of standard deviations for values near the start of the test limit Hct calculation accuracy for the first ~10 s of the test. After ~22 s all Hct measurements stabilize close to their nominal value. Fig. 7b shows the time at which Hct measurements reach within 1% Hct of the nominal value. Calculation of whole blood with 45% Hct is seen to require a minimum of 22 s in order to accurately calculate the Hct value, while for 40% Hct measurement an accurate threshold is reached after only 10 s. The longest detection time, 22 s, is set as a limiting factor for the LFTA to make an accurate measurement and display the result to the
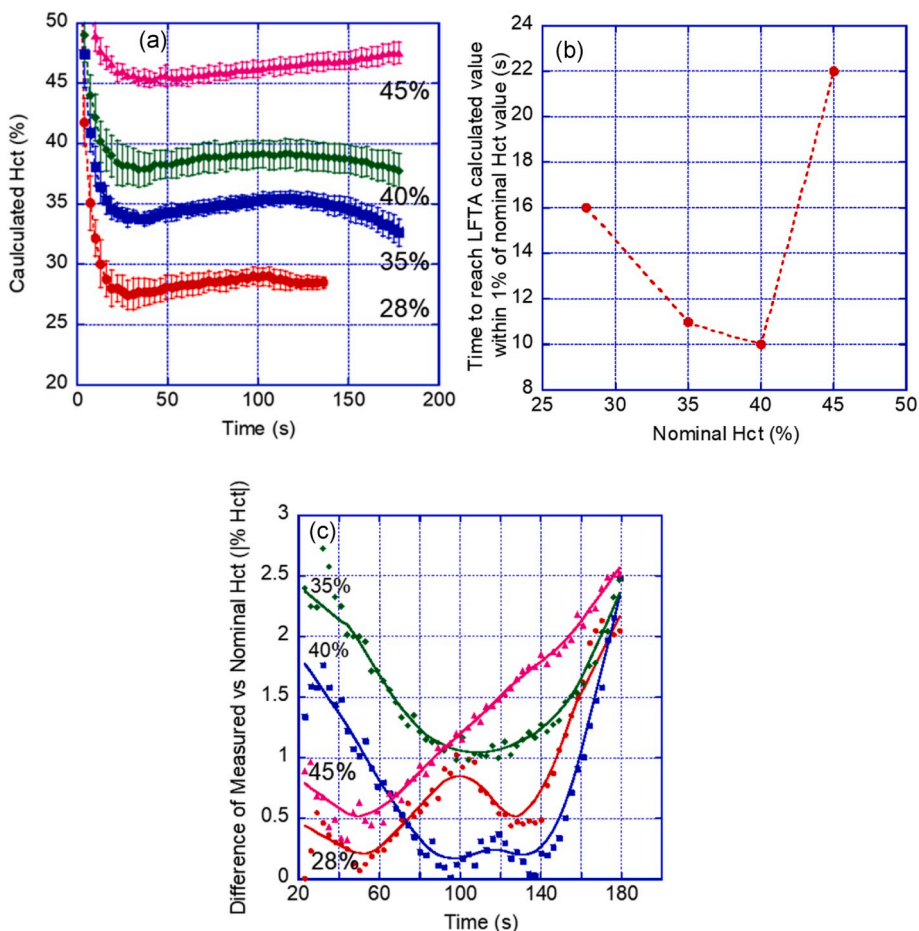

Fig. 7. LFTA algorithm calculated Hct values for nominal Hct values of 28, 35, 40, and 45%: (a) calculated Hct vs. time; (b) detection time required to produce minimum accurate (~1% Hct) LFTA value for each nominal Hct value; (c) difference between measured and nominal Hct% value as a function of time.

user.

Fig. 7c highlights the measurement error between the calculated and nominal Hct values after 22s. The greatest deviation from nominal value is found to be 2.8% Hct, with typical error less than 2% Hct. Fig. 7c also shows that the measured values increase in all cases for time greater than 120s. This is due to the decreasing linearity of the relationship between calculated Hct% and distance after 120 s, as shown in Fig. 6b.

Fig. 8 compares the actual Hct values measured with the hematocrit centrifuge vs Hct measurements obtained with the LFTA (data points and dashed blue line) at the 22 s mark. An ideal 1:1 relationship (red line) is shown to illustrate deviation from the conventional centrifugation measurement. The measured value of 28% Hct whole blood was found to be within 0.006% Hct of the nominal value. The largest deviation between measured and nominal values of only 2.4% Hct occurred for the 40% Hct measurement. A linear fit of the LFTA measurements (dashed blue line) was performed, yielding an R value of 0.98. The slope of LFTA measurements is 1.0171, only a 1.71% difference from the ideal slope of 1.0 (where the centrifuge and the LFTA app values are identical).

Thus, the LFTA is shown to not only provide accurate quantitative Hct measurement but do so substantially faster than conventional measurement of flow-based devices. Use of the LFTA in conjunction with nrLFAs can help patients to accurately, conveniently, and quickly keep track of their Hct.

Potential improvements to the system could be made through reducing the signal noise during the first 15 s of Hct testing, as well as reducing measurement drift during longer test times. Reduction of early signal noise could potentially be achieved through higher resolution video acquisition and analysis as well as more frequent measurement of the flow distance. Measurement drift during long test time is a result of the curve fitting used to calculate Hct. This could be reduced by curve fitting using a larger sample set.

4. Conclusions

Utilizing the camera and image processing capabilities built into a smartphone, the LFTA acted as a handheld device to measure flow rates through an LFA. Our results have shown quantitative measurement of blood flow rate through commercially available LFA cassettes as well as accurate Hct values without the need for modifications or custom hardware. Whole blood with Hct values of 28, 35, 40, and 45% were measured using the LFTA. The results showed a clear trend consistent with previous work. Whole blood hematocrit values with 1% accuracy were rapidly calculated using the smartphone in as little as 10 s and no more than 22s.

To our knowledge, this is the first smartphone-based PoC system to measure fluid flow distance through an LFA cassette and to calculate Hct without the need of external hardware.

Removing the need of external hardware allows the LFTA platform to more easily be used in a PoC setting. The absence of external hardware also enables the system to be rapidly deployed anywhere the nrLFA test is being performed, simply by downloading the app. The simple path for this operational enhancement has the potential to lead to faster and higher adoption rates compared to other phone based PoC systems. Higher usage of the LFTA in conjunction with the nrLFA could improve patient test reliability and accuracy, helping them perform necessary tests regardless of location. However, an enclosure on the application could be used to improve consistency in lighting and potentially increase detection of blood flow in the nrLFA in extreme lighting conditions. An origami style enclosure similar to that used by Yang et al. could be used for the enclosure.

The methods used in the LFTA are not limited to the measurement of Hct concentration in blood. With recalibration, INR could be calculated based on RBC flow rate. In theory, any flow-based test could be made quantitative using the LFTA. This includes changes to the cassette, flow medium, analyte fluid, or calculated parameter. The techniques used
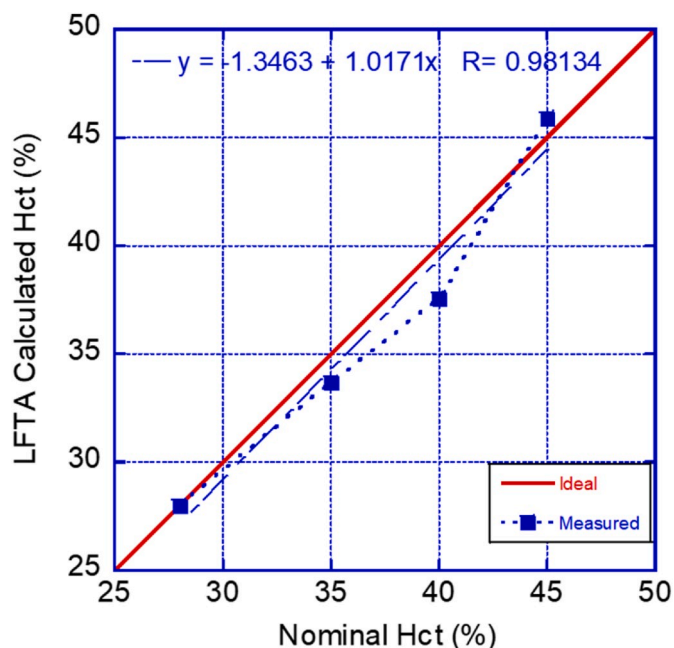

Fig. 8. LFTA measured Hct values at 22s test time compared to nominal blood Hct values. Dashed blue line is a curve fit of measured Hct values. Solid red line represents the ideal 1:1 case. (For interpretation of the references to color in this figure legend, the reader is referred to the Web version of this article.)

could also be applied to non-LFA distance-based measurements, such as those in microfluidic chips.

Declaration of competing interest

The authors declare that they have no known competing financial interests or personal relationships that could have appeared to influence the work reported in this paper.

CRediT authorship contribution statement

Eric Frantz: Investigation, Writing - original draft. **Hua Li:** Methodology. **Andrew J. Steckl:** Conceptualization, Writing - review & editing.

Acknowledgements/Funding

Appendix A. Supplementary data

Supplementary data to this article can be found online at https://doi. org/10.1016/j.bios.2020.112300.

References

AbingdonHealth, 2019. ADxLR5® Reader System. Abingdon Health. https://www. abingdonhealth.com.

Axxin, 2019. AX-2X-S Lateral Flow Reader. Axxin. https://www.axxin.com/.

Bahadır, E.B., Sezgintürk, M.K., 2016. Lateral flow assays: principles, designs and labels. Trac. Trends Anal. Chem. 82, 286–306.

Berry, S.B., Fernandes, S.C., Rajaratnam, A., DeChiara, N.S., Mace, C.R., 2016. Measurement of the hematocrit using paper-based microfluidic devices. Lab Chip 16 (19), 3689–3694.

Deng, W., Dou, Y., Song, P., Xu, H., Aldalbahi, A., Chen, N., El-Sayed, N.N., Gao, J., Lu, J., Song, S., Zuo, X., 2016. Lab on smartphone with interfaced electrochemical chips for on-site gender verification. J. Electroanal. Chem. 777, 117–122.

Ding, J., Yu, N., Wang, X., Qin, W., 2018. Sequential and selective detection of two molecules with a single solid-contact chronopotentiometric ion-selective electrode. Anal. Chem. 90 (3), 1734–1739.

Eltzov, E., Guttel, S., Low Yuen Kei, A., Sinawang, P.D., Ionescu, R.E., Marks, R.S., 2015. Lateral flow immunoassays - from paper strip to smartphone technology. Electroanalysis 27 (9), 2116–2130.

Erenas, M.M., Carrillo-Aguilera, B., Cantrell, K., Gonzalez-Chocano, S., de Vargas-Sansalvador, I.M.P., de Orbe-Payá, I., Capitan-Vallvey, L.F., 2019. Real time monitoring of glucose in whole blood by smartphone. Biosens. Bioelectron. 136, 47–52.

Escobedo, P., Erenas, M.M., Martínez-Olmos, A., Carvajal, M.A., Gonzalez-Chocano, S., Capitán-Vallvey, L.F., Palma, A.J., 2019. General-purpose passive wireless point–of–care platform based on smartphone. Biosens. Bioelectron. 111360.

Ghosh, S., Aggarwal, K., Vinitha, T., Nguyen, T., Han, J., Ahn, C.H., 2020. A new microchannel capillary flow assay (MCFA) platform with lyophilized chemiluminescence reagents for a smartphone-based POCT detecting malaria. Microsyst. Nanoeng. 6 (1), 1–18.

Guan, L., Tian, J., Cao, R., Li, M., Cai, Z., Shen, W., 2014. Barcode-like paper sensor for smartphone diagnostics: an application of blood typing. Anal. Chem. 86 (22), 11362–11367.

Han, J., Zhang, L., Hu, L., Xing, K., Lu, X., Huang, Y., Zhang, J., Lai, W., Chen, T., 2018. Nanozyme-based lateral flow assay for the sensitive detection of Escherichia coli O157: H7 in milk. J. Dairy Sci. 101 (7), 5770–5779.

Hegener, M.A., Li, H., Han, D., Steckl, A.J., Pauletti, G.M., 2017. Point-of-care coagulation monitoring: first clinical experience using a paper-based lateral flow diagnostic device. Biomed. Microdevices 19 (3), 64.

Hou, Y., Wang, K., Xiao, K., Qin, W., Lu, W., Tao, W., Cui, D., 2017. Smartphone-based dual-modality imaging system for quantitative detection of color or fluorescent lateral flow immunochromatographic strips. Nanoscale Res. Lett. 12 (1), 291.

Insights, F.M., 2016. Fertility and pregnancy rapid test kits market: high acceptance of digital pregnancy devices to witness rapid growth during forecast period: global industry analysis and opportunity assessment 2016 - 2026. Future Market Insights. https://www.futuremarketinsights.com/reports/fertility-and-pregnancy-rapid-tests-market.

Kanchi, S., Sabela, M.I., Mdluli, P.S., Inamuddin, Bisetty, K., 2018. Smartphone based bioanalytical and diagnosis applications: a review. Biosens. Bioelectron. 102, 136–149.

Khan, M.S., Thouas, G., Shen, W., Whyte, G., Garnier, G., 2010. Paper diagnostic for instantaneous blood typing. Anal. Chem. 82 (10), 4158–4164.

Kim, S.C., Jalal, U.M., Im, S.B., Ko, S., Shim, J.S., 2017. A smartphone-based optical platform for colorimetric analysis of microfluidic device. Sensor. Actuator. B Chem. 239, 52–59.

Koczula, Katarzyna M., Gallotta, A., 2016. Lateral flow assays. Essays Biochem. 60 (1), 111–120.

Laksanasopin, T., Guo, T.W., Nayak, S., Sridhara, A.A., Xie, S., Olowookere, O.O., Cadinu, P., Meng, F., Chee, N.H., Kim, J., 2015. A smartphone dongle for diagnosis of infectious diseases at the point of care. Sci. Transl. Med. 7 (273), 273re271-273re271.

Li, H., Han, D., Hegener, M.A., Pauletti, G.M., Steckl, A.J., 2017. Flow reproducibility of whole blood and other bodily fluids in simplified no reaction lateral flow assay devices. Biomicrofluidics 11 (2), 024116.

Li, H., Han, D., Pauletti, G., Hegener, M.A., Steckl, A.J., 2018a. Correcting the effect of hematocrit in whole blood coagulation analysis on paper-based lateral flow device. Anal. Methods 10 (24), 2869–2874.

Li, H., Han, D., Pauletti, G.M., Steckl, A.J., 2014. Blood coagulation screening using a paper-based microfluidic lateral flow device. Lab Chip 14 (20), 4035–4041.

Li, H., Han, D., Pauletti, G.M., Steckl, A.J., 2018b. Engineering a simple lateral flow device for animal blood coagulation monitoring. Biomicrofluidics 12 (1), 014110.

Li, H., Steckl, A.J., 2018. Paper microfluidics for point-of-care blood-based analysis and diagnostics. Anal. Chem. 91 (1), 352–371.

Lopez-Ruiz, N., Curto, V.F., Erenas, M.M., Benito-Lopez, F., Diamond, D., Palma, A.J., Capitan-Vallvey, L.F., 2014. Smartphone-based simultaneous pH and nitrite colorimetric determination for paper microfluidic devices. Anal. Chem. 86 (19), 9554–9562.

Noiphung, J., Talalak, K., Hongwarittorrn, I., Pupinyo, N., Thirabowonkitphithan, P., Laiwattanapaisal, W., 2015. A novel paper-based assay for the simultaneous determination of Rh typing and forward and reverse ABO blood groups. Biosens. Bioelectron. 67 (Suppl. C), 485–489.

Novarum, 2018. Novarum Mobile Reader Solutions. Novarum™ DX Ltd.

O'Farrell, B., 2009. Evolution in lateral flow–based immunoassay systems. In: Wong, R., Tse, H. (Eds.), Lateral Flow Immunoassay. Humana Press, Totowa, NJ, pp. 1–33.

Rohrman, B.A., Leautaud, V., Molyneux, E., Richards-Kortum, R.R., 2012. A lateral flow assay for quantitative detection of amplified HIV-1 RNA. PloS One 7 (9), e45611.

Sajid, M., Kawde, A.-N., Daud, M., 2015. Designs, formats and applications of lateral flow assay: a literature review. J. Saudi Chem. Soc. 19 (6), 689–705.

Srinivasan, B., O'Dell, D., Finkelstein, J.L., Lee, S., Erickson, D., Mehta, S., 2018. ironPhone: mobile device-coupled point-of-care diagnostics for assessment of iron status by quantification of serum ferritin. Biosens. Bioelectron. 99, 115–121.

Steckl, A.J., Ray, P., 2018. Stress biomarkers in biological fluids and their point-of-use detection. ACS Sens. 3 (10), 2025–2044.

van Amerongen, A., Veen, J., Arends, H.A., Koets, M., 2018. Lateral Flow Immunoassays. Handbook of Immunoassay Technologies. Elsevier, pp. 157–182.

Vashist, S.K., Luppa, P.B., Yeo, L.Y., Ozcan, A., Luong, J.H., 2015. Emerging technologies for next-generation point-of-care testing. Trends Biotechnol. 33 (11), 692–705.

Venkatraman, V., Liedert, R., Kozak, K., Steckl, A.J., 2016. Integrated NFC power source for zero on-board power in fluorescent paper-based lateral flow immunoassays. Flex. Print. Electr. 1 (4), 044001.

Yang, J.-S., Shin, J., Choi, S., Jung, H.-I., 2017. Smartphone Diagnostics Unit (SDU) for the assessment of human stress and inflammation level assisted by biomarker ink, fountain pen, and origami holder for strip biosensor. Sensor. Actuator. B Chem. 241, 80–84.

Zhan, S., Wu, Y., Wang, L., Zhan, X., Zhou, P., 2016. A mini-review on functional nucleic acids-based heavy metal ion detection. Biosens. Bioelectron. 86, 353–368.

Zhang, L., Yang, W., Yang, Y., Liu, H., Gu, Z., 2015. Smartphone-based point-of-care testing of salivary alpha-amylase for personal psychological measurement. Analyst 140 (21), 7399–7406.